

Silver nanostructured surfaces prepared by MAPLE for biofilm prevention

Oana Fufă^{1,2}, Ecaterina Andronescu¹, Valentina Grumezescu^{1,2}, Alina Maria Holban^{1,3}, Laurențiu Mogoantă⁴, George Dan Mogoșanu⁵, Gabriel Socol², Florin Iordache⁶, Mariana Carmen Chifiriuc^{3,7}, Alexandru Mihai Grumezescu^{1,*}

¹Department of Science and Engineering of Oxide Materials and Nanomaterials, Faculty of Applied Chemistry and Materials Science, University Politehnica of Bucharest, 1-7 Polizu Street, 011061 Bucharest, Romania

²Lasers Department, National Institute for Lasers, Plasma & Radiation Physics, P.O. Box MG-36, Magurele, Bucharest, Romania

³Microbiology Immunology Department, Faculty of Biology, University of Bucharest, 1-3 Portocalilor Lane, Sector 5, 77206 Bucharest, Romania⁴Research Center for Microscopic Morphology and Immunology, University of Medicine and Pharmacy of Craiova, 2 Petru Rareș Street, 200349 Craiova, Romania

⁵Department of Pharmacognosy & Phytotherapy, Faculty of Pharmacy, University of Medicine and Pharmacy of Craiova, 2 Petru Rareș Street, 200349 Craiova, Romania

⁶Department of Fetal and Adult Stem Cell Therapy, "Nicolae Simionescu" Institute of Cellular Biology and Pathology of Romanian Academy, 8 B.P. Hasdeu, 050568 Bucharest, Romania

⁷Research Institute of the University of Bucharest, Spl. Independentei 91-95, Bucharest, Romania

*corresponding author e-mail address: grumezescu@yahoo.com

ABSTRACT

One of the current challenging trends in modern healthcare practice is to diminish the number and severity of nosocomial infections. Considering the increased incidence of medical devices associated infections produced by opportunistic pathogens, novel strategies to develop medical devices with surfaces resistant to microbial colonization are needed. Thus, the aim of this research was to produce improved coatings with higher anti-adherence and antibiofilm properties, by superficial surface modification of such devices using the novel MAPLE technique to deposit thin layers of silver nanoparticles. Silver nanoparticles were prepared by using a facile wet chemical route and the obtained silver nanopowder was afterwards used via laser processing to produce thin homogenous inorganic layers onto the considered medical devices. The as-produced surfaces were characterized and their antibiofilm potential was investigated both against Gram-positive and Gram-negative bacterial strains. The promising results regarding higher and longer resistance to bacterial contamination, as well as good biocompatibility reveal the potential of the MAPLE technique for optimizing the surface of day-to-day medical care devices.

1. INTRODUCTION

The current requirements of modern world regarding the quality of healthcare practices and the implementation of the *personalized medicine* concept are still challenged by nosocomial infections, which may oppressively impact the outcome of the therapeutic strategy [1, 2], especially when taking into account the alarming increase in the number bacterial strains which developed drug resistance, due to the improper or irrational use of antibiotics [3,4]. Therefore, alternative strategies to prevent and combat microbial contamination are needed.

Regarding the unconventional strategies to fight against microbes, the worldwide community turned its attention towards the novel engineered nanosized systems, since they possess unique and attractive features. The physicochemical versatility of bulk silver, its acknowledged antimicrobial activity and the tremendous latest nanotechnology-related opportunities represented essential criteria towards engineering novel silver-based nanomaterials. Among the silver nano-related structures – which include nanowires [5,6], nanotubes [7,8], nanorods [9,10], nanobars [11,12] and nanoparticles – the most explored nanosystems are the silver nanoparticles (AgNPs) [13,14].

When considering the fundamentals of novel attractive and innovative technologies on bulk silver and silver-containing compounds, various strategies to synthesize high purity and tunable AgNPs were successfully developed: (a) the physical synthesis approach involves concurrent evaporation-condensation

phenomena of bulk silver by means of various external energies [15,16]; (b) the chemical synthesis relies on metallic precursors degradation by electrochemical means in presence of reducing agents and stabilizers [17,18,19]; (c) the physicochemical synthesis specifically uses external energies to guide the nucleation, incubation and maturation processes within the particle formation [20,21,22,23,24]; (d) the biological synthesis focuses on the exploitation of microbial bioreduction mechanisms and of phytochemicals [25,26,27,28,29,30,31].

Given the size-dependent properties of silver nanoparticles – in terms of unique optical properties and electrical conductivity, chemical stability and catalytic activity, antibacterial, antifungal, antiviral and anti-inflammatory activity – promising results with respect to the biomedical applications of AgNPs were reported, including antimicrobial applications [32,33,34], drug delivery [35,36,37], biosensing [38,39,40], medical imaging [41,42,43] and tissue engineering [44,45,46].

The antimicrobial properties of silver nanoparticles strongly recommend such structures for designing novel materials with improved microbial resistance, either in terms of preventing contamination or combating microbial colonization. Thus, various physical and chemical techniques have been successfully used to develop thin silver-based nanostructures onto the surface of the microbial susceptible medical devices [47,48].

Therefore of the aim of this paper was to fabricate silver-based nanostructured coatings deposited on the surface of venous central catheters by using the MAPLE technique (a newly pulsed-assisted deposition strategy which enables a “soft” and high

quality transfer of the target material onto the concerned substrates, but also a facile control over the experimental parameters).

2. EXPERIMENTAL SECTION

2.1. Materials.

The silver nitrate (AgNO_3), D-glucose ($\text{C}_6\text{H}_{12}\text{O}_6$), sodium hydroxide (NaOH), sodium stearate ($\text{C}_{18}\text{H}_{35}\text{NaO}_2$), sodium chloride (NaCl), acetone ($\text{C}_3\text{H}_6\text{O}$) and chloroform (CHCl_3) used for wet chemical synthesis, stabilization and dispersion of silver nanoparticles, as well as dimethyl sulfoxide DMSO ($(\text{CH}_3)_2\text{SO}$), used for MAPLE targets were purchased from Sigma-Aldrich.

The medical devices consisted in polyvinyl chloride (PVC) central venous catheters. Also, side polished silicon (Si) (100) and glass were pelliculized by MAPLE, as suitable substrates for IRM, respectively AFM and SEM analyses.

2.2. Methods.

2.2.1. AgNPs synthesis.

The experimental synthesis of silver nanoparticles required the use of two distinctive aqueous solutions. Firstly, the metallic precursor solution was obtained by dissolving 0.1 g of AgNO_3 in 100 mL of ultrapure water. Secondly, the stabilizer solution was prepared by dissolving 0.5 g of $\text{C}_{18}\text{H}_{35}\text{NaO}_2$, 1 g of $\text{C}_6\text{H}_{12}\text{O}_6$ and 4 g of NaOH in 400 mL of ultrapure water, under magnetic stirring at 80°C . Thereafter, the silver nitrate solution was dropwise added to the surfactant solution, under continuous stirring. 30 g of NaCl were then added, in order to destabilize the obtained suspension and the filtration process allowed us to successfully collect the synthesized AgNPs. Afterwards, the silver particles were subjected to a triple washing treatment with acetone and dried at room temperature. A small amount of the obtained powder was subsequently investigated by using various analytical methods, while a large amount of the synthesized particles was further suspended in chloroform to obtain the AgNPs-based nanostructured coatings.

2.2.2. AgNPs-based nanostructured coatings fabrication.

In order to obtain the MAPLE target, a 0.7% solution consisting in silver nanoparticles and DMSO was prepared and frozen with liquid nitrogen, by using a 30 minutes treatment. Before deposition, several venous catheter sections with 1 cm length were obtained, successively cleaned with acetone, ethanol and deionized water for 15 minutes in an ultrasonic bath and dried in a stream of high purity nitrogen. The same cleaning treatment was also applied to glass and silicon substrates. In all experiments, the AgNPs-containing targets were placed at 4 cm distance from substrates and the depositions were performed by using a KrF* excimer laser beam ($\lambda = 248 \text{ nm}$, $\tau_{\text{FWHM}} = 25 \text{ ns}$), produced by a COMPexPro 205 Lambda Physics-Coherent source. The frozen targets were continuously rotated with 0.4 Hz frequency during all depositions and were irradiated at room temperature with three experimental laser fluences (400, 500 and 600 mJ/cm^2), by applying 30,000 laser pulses.

2.2.3. X-ray diffraction (XRD).

Relevant information with respect to the purity and crystallinity of the AgNPs powder were obtained by using a Shimadzu XRD 6000 diffractometer. Thus, a small amount of the powdery AgNPs-based sample was investigated by using the $\text{Cu}_{K\alpha}$ radiation with $\lambda = 1,056 \text{ \AA}$ of the selected instrument, which enabled the scanning of the sample by using 2θ Bragg scattering angles between 10° and 80° .

2.2.4. Transmission electron microscopy (TEM).

The intimate microstructure of the AgNPs-based powder was examined by using a Tecnai™ G2 F30 S-TWIN high resolution transmission electron microscope from FEI Company (Oregon, USA) equipped with a SAED (selected area electron diffraction) instrument. A small amount of the silver-based sample was dispersed in absolute ethanol under ultrasonic conditions for 15 minutes, then placed on a holey carbon-coated copper grid and dried at room temperature. The microscope operated in transmission mode at 300 kV with point resolution of 2 \AA and line resolution of 1 \AA .

2.2.5. Infra-Red Mapping (IRM).

Relevant data with respect to structural homogeneity and chemical composition of the MAPLE produced films were obtained by using a Nicolet iN10 MX FT-IR microscope with a MCT liquid nitrogen cooled detector (Thermo Nicolet). The IR mapping was recorded in reflection mode, by using the measurement range of $4,000\text{-}600 \text{ cm}^{-1}$ at 4 cm^{-1} resolution. 32 distinctive scans were recorded, co-added and converted to absorbance for each spectrum by using the OmnicPicta software (Thermo Scientific).

2.2.6. Atomic force microscopy (AFM).

The roughness and topography-related aspects of the AgNPs-based deposited coating were experimentally evaluated by using a 4000 Multiview System which enables multiprobe analysis by atomic force microscopy means, purchased from Nanonics Imaging Ltd. Company (Israel). The scan areas ($10 \mu\text{m} \times 10 \mu\text{m}$) were analyzed by using 256 distinctive scans recorded by the tapping-mode working microscope.

2.2.7. Scanning electron microscopy (SEM).

Prior to SEM analysis, the experimental coatings deposited onto Si (100) substrates were cut by using a diamond disc. The morphology and dimension of the produced thin coatings were thus evaluated in cross section, by using the secondary electron beam with 30 keV energy of a scanning electron microscope equipped with precise electronic microprobe, purchased from FEI Company (Oregon, USA).

2.2.8. *In vivo* biodistribution.

In order to experimentally evaluate the *in vivo* distribution of the synthesized silver nanoparticles, two albino mice were

intraperitoneally inoculated with 200 μL of AgNPs suspension of 1 mg/mL concentration that was prepared by dispersing the particles in ultrapure water and further subjecting the mixture to a 30 min UV sterilizing treatment. Two distinctive albino mice were inoculated with the same amount of saline solution (as negative control). At 7 and 14 days of experimental treatment, the animals were sacrificed after ethyl ether general anesthesia, in order to harvest the vital organs. The harvested organs were subsequently treated with phosphate buffered saline (PBS) for blood removal and preserved in 10% formaldehyde solution for 72 hours, at room temperature. The as-treated tissue samples were further accordingly prepared for paraffin processing and treated with hematoxylin and eosin (H&E) staining, with the purpose of following histological examination. The histological examination of the prepared microscope slides was made by using a Nikon Eclipse 55i binocular microscope purchased from Apidrag company (Bucharest, Romania), while the acquisition of images was performed by coupling a high quality and resolution Nikon DS-Fi1 camera to the optical microscope and by using the Image Pro Plus 6.0 software purchased from Media Cybernetics Company (Marlow, Buckinghamshire, UK).

3. RESULTS SECTION

The nanosized silver-based particles were synthesized in this study using a facile wet chemical synthesis method, starting from a silver metallic solution and a fatty acid-based stabilizer solution. During the stirring-assisted synthesis process, the color of the obtained aqueous solution rapidly changed in brownish green, witnessing the physicochemical processes leading to silver nanoparticles formation [49,50,51]. The as-synthesized powdery sample was further collected and investigated by various analytical means.

3.1. XRD

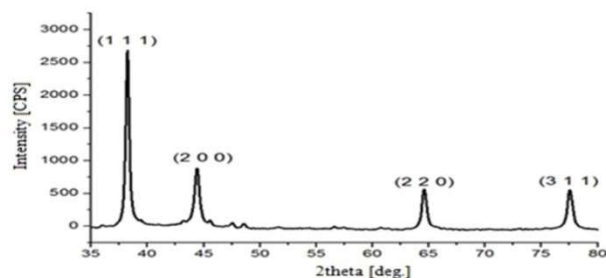


Figure 1. XRD pattern of the synthesized silver-based powder.

When considering the XRD pattern showed in Figure 1, one can clearly see distinguishable diffraction interferences with minimal background noise, which may be assigned to high purity silver-based powder. On the other hand, regarding the intense diffraction peaks identified for 2θ diffraction angles of 38.02° , 44.2° , 64.3° and 77.39° and the American Society for Testing and Materials available charts, we were able to specifically identify the (1 1 1), (2 0 0), (2 2 0) and (3 1 1) diffraction planes that are specific for crystallized silver in face-centered cubic system.

3.2. IR

The IR spectra were obtained for both pure sodium stearate and sodium stearate-stabilized silver nanoparticles. As the obtained spectra revealed, the infrared absorption peaks of the

2.2.9. *In vitro* evaluation.

The anti-bacterial and anti-biofilm potential of the experimentally modified medical devices was *in vitro* assessed in the presence of uncoated and AgNPs-coated catheter sections against three bacterial pathogens, namely *Escherichia coli*, *Pseudomonas aeruginosa* and *Staphylococcus aureus*. The uncoated and coated catheter sections were placed in 6 well plates, and 2 mL of microbial suspension of 0.5 McFarland standard density ($1.5 \cdot 10^8$ CFU/mL) prepared from each bacterial strain were inoculated in each well and further incubated for 24 hours at 37°C . Thereafter, the culture medium was removed and the specimens were washed with sterile PBS (phosphate buffered saline). The catheter sections were subsequently placed in fresh medium and incubated for other additional 24, 48 and 72 hours. After each incubation time, the medical devices samples were gently washed with sterile PBS and placed in 1.5 mL centrifuge tubes containing 750 μL of PBS. Further, the as obtained specimens were vigorously centrifuged for 30 seconds and sonicated for 10 seconds. Serial ten-fold dilutions were performed from the recovered suspensions and distributed in fix amounts on Luria Broth agar plates, for viable cell counts assay. All the experiments were performed in triplicate and repeated in three separate occasions.

organic fatty acid have not been altered during the synthesis process, which means that no strong chemical interactions occurred, but surface physical and weak chemical interactions. However, due to the weak chemical interactions established between the inorganic and organic component, some amplitude and shape-related changes were observed with respect to the absorption interferences. The specific presence of the fatty acid within the synthesized nanostructures is confirmed by the absorption bands that correspond to 2919 cm^{-1} ($-\text{CH}_2-$ asymmetric stretching vibrations), 2850 cm^{-1} ($-\text{CH}_2-$ symmetric stretching vibrations), 1558 cm^{-1} ($-\text{COOH}$ asymmetric stretching vibrations), 1444 and 1422 cm^{-1} ($-\text{COO}^-$ symmetric stretching vibrations) wavelength. The IR spectra were presented elsewhere [52]. The infrared absorption spectra confirmed the formation of pure physical and weak chemical interactions between the two components, suggesting rather the image of silver nanoparticles coated with a superficial thin organic shell [53].

3.3. TGA

According to the obtained derivatogram, the DTA graph marks a weak endothermic process associated with a mass loss of 1.53% between 30°C and 170°C , which may be assigned to humidity water evaporation. The two exothermic phenomena emphasized in the temperature range of 200 – 350°C are accompanied by an 18% mass loss and may be associated with the crystallization process of AgNPs. The last thermal range, comprised between 400°C and 500°C , shows two distinctive exothermic phenomena with a corresponding mass loss of approximate 12%, which may correspond to thermal disintegration of the fatty acid. Thus, the total mass loss reported for the applied thermal treatment has an approximate value of 41%, so one can assume that the mass ratio of the inorganic and organic components within the analyzed powder is 60/40. The thermogram corresponding to the silver-based powdery sample was presented

elsewhere [52]. Regarding the composition of the synthesized silver-based sample, the TGA data showed that the obtained particles possess a major inorganic component, but also a considerable organic component (the 60 % wt. were assigned to the metallic silver, while the 40% w.t. were assigned to stabilizer fatty acid). Thus, the previously assumed core-shell structure of the synthesized particles was confirmed, the stearate ions being specifically adsorbed onto the highly reactive surface of the AgNPs.

3.4. TEM

The obtained TEM images captured in Figure 2 (a and b) allow us to acquire significant data regarding the morphology and size of the synthesized silver nanoparticles. One can thus notice that the obtained particles have a reduced tendency to form agglomerated structures, thanks to the fatty acid stabilizing agent. The selected synthesis method allowed us to obtain spherical AgNPs with dimensional range below 20 nm. Considering the TEM micrographs, we were able to experimentally determine the average grain size (7.95 ± 2.55 nm).

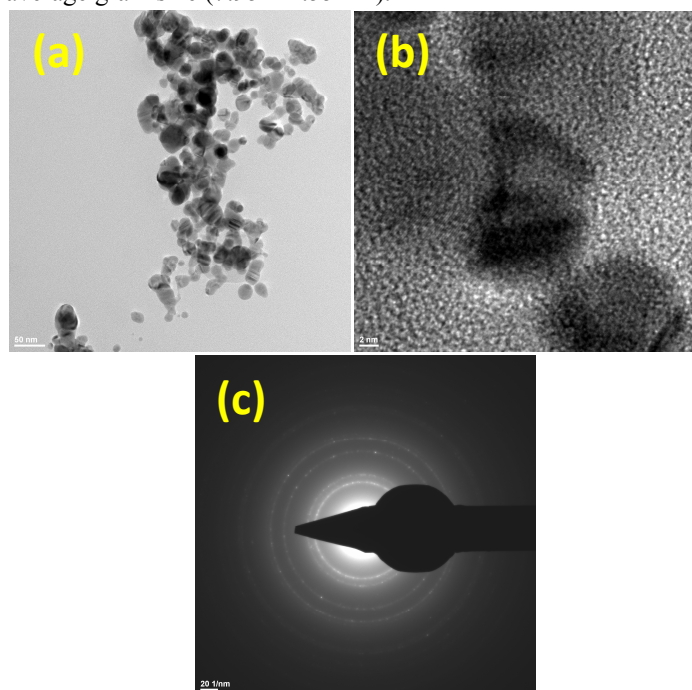


Figure 2. HR-TEM images of silver particles (a,b) and SAED pattern (c).

Also, the specific concentric distribution of diffraction planes within the SAED image observed in Figure 2c confirmed the previous data with respect to the (111), (200) and (311) diffraction planes of face-centered cubic crystalline structure of spherical silver nanoparticles, that were obtained by XRD means.

3.5. IRM

The IRM analysis performed for the experimentally obtained silver-based films enabled us to study the structural homogeneity and the chemical composition within the coatings deposited onto glass substrates, when considering three experimental deposition conditions. The infrared mapping of the experimentally produced silver-based films was performed by considering the asymmetric and symmetric stretching vibrations within the specific carboxyl groups of the fatty acid. The distribution homogeneity and the chemical integrity of the concerned functional group within the experimental films are shown in Figure 3. By relating the IR maps to the infrared

absorption spectra of various random spots within the coating, we estimated that the lowest degradation of the concerned functional group occurs when using the 600 mJ/cm^2 laser fluence. One can preliminarily assume that the suitable conditions to produce high quality AgNPs-based coatings correspond to the last experimental version.

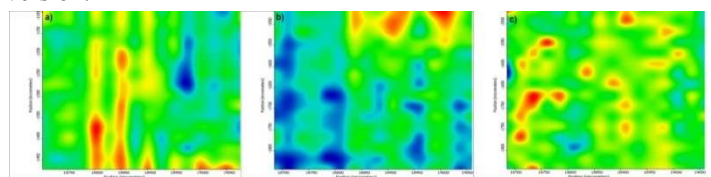


Figure 3. IR maps of AgNPs-based coatings obtained by the MAPLE technique, by using various laser fluences: 400 mJ/cm^2 (a), 500 mJ/cm^2 (b), 600 mJ/cm^2 (c).

3.6. AFM

As the AFM data from Figure 4 shows, silver-based nanosized films can be successfully produced by using the MAPLE technique. The AFM topography images rather revealed the significant roughness of the silver-based films deposited onto the silicon substrates. However one can notice that significant film degradation occurs when using lower laser fluences (the identified dark dominant regions are broader). The third experimental deposition, corresponding to 600 mJ/cm^2 laser fluence, reveals rather an uniform and homogenous AgNPs-based film, with no critical alterations in terms of structural integrity. Given the as-obtained data with respect to the uniformity and structural integrity, the AFM results confirmed our previous assumption with respect to the potential use of 600 mJ/cm^2 laser fluence to experimentally produce silver-based coatings onto the PVC venous catheter sections.

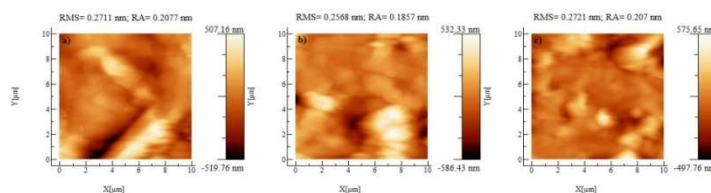


Figure 4. AFM images of AgNPs-based coatings obtained by the MAPLE technique, by using various laser fluences: 400 mJ/cm^2 (a), 500 mJ/cm^2 (b), 600 mJ/cm^2 (c). RMS – root mean square roughness; RA – roughness average.

3.7. SEM

When considering the SEM micrograph within Figure 5, one can observe the auspicious uniformity of the AgNPs-based film deposited onto the silicon substrate, but one can also remark the intrinsic roughness of the obtained surface. Given the physically-guided interactions between the Si substrate and the irradiation resulting plasma, the detached fragments of the frozen target (including silver nanoparticles and ions, but also organic solvent compounds) rearranged into rather embossed structures. Also, considering the specific SEM software, we could experimentally determine an approximate 500 nm thickness of the silver-based nanostructured coating.

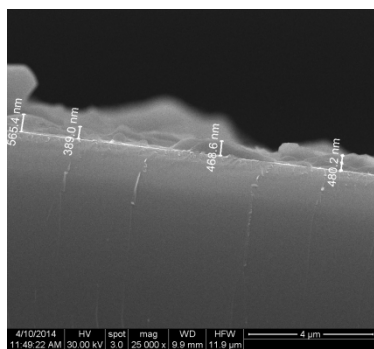


Figure 5. SEM cross section image of the AgNPs-based coating obtained by MAPLE technique, using a laser fluence of 600 mJ/cm^2 , at $25,000\times$ magnification.

3.8. *In vivo* biodistribution

The histological examination of brain, myocardium, pancreas, liver, lung and kidney tissues revealed no structural modifications, functional alterations or inflammatory signs after 7 days or 14 days of experimental treatment with silver nanoparticles. Regarding the brain tissue sample, one could clearly distinguish three specific regions of cerebral cortex (the molecular layer, the outer granular layer and the outer pyramidal cell layer). Also, typical features assigned to the abundant glial cells were distinguished: prominent euchromatic spherical nuclei with typical vesicular aspect that possess visible nucleoli within an eosinophilic cytoplasmic mass. When considering the normal histological aspects specifically identified within the brain, one can assume that the inoculated AgNPs suspension does not cross the blood-brain barrier.

The myocardial tissue samples revealed normal striated cardiac muscle fibers, with specific heterochromatic round-oval nuclei. Few longitudinally captured capillaries presented a significant amount of erythrocytes. Regarding the pancreatic tissue samples, pancreatic acini consisting in a single layer of cuboidal epithelium cells with spherical nuclei that corresponds to the exocrine pancreas were observed. The highly polarized cells (with eosinophilic aspect at the secretory pole and basophilic aspect at the basal pole) suggested a normal secretory activity. Also, the pale epithelial cells with single central oval nuclei specifically corresponded to the endocrine pancreas structure. With respect to the myocardial and the pancreatic tissues – which do not possess native immune structures – the observed histological aspects were normal and no tissue damage, inflammatory infiltrate or inorganic deposits were noticed. One can assume that the administration of silver-based nanosystems through the bloodstream is not followed by cellular internalization and subsequent cell injury.

The liver tissue sections revealed polyhedral shaped hepatocytes (with prominent spherical euchromatic nuclei) disposed within specific highly arranged cords that delimit sinusoidal capillaries with erythrocyte content. Also, a significant amount of red blood cells were noticed within the centrilobular veins captured in cross section. With respect to the pulmonary tissue microscopic slides, one could clearly distinguish type I pneumocytes (flattened squamous cells which define the alveolar sacs) and type II alveolocytes (spherical prominent cells with foamy cytoplasm and unique round nuclei located within the inter-alveolar septa). Alveolar capillaries with significant normal red

blood cell content could be observed near the alveolar septa. The histological aspects observed for the hepatic and pulmonary tissue samples are also normal, with no relevant signs of any activity within the hepatic Kupffer cells or pulmonary macrophage cells.

Within the renal cortex tissue samples, the renal corpuscles marked off between the visceral and parietal layers of Bowman's capsule possessed specific intraglomerular mesangial cells with singular prominent round-oval nuclei. Also, it was clearly noticed that the proximal convoluted (single layered cubic epithelial regions with specific narrower lumen) and distal convoluted (single layered cubic epithelial regions with specific wider lumen) renal tubules possessed typical histological aspects. Within the captured renal capillaries one could notice a significant amount of histological normal erythrocytes. The histological aspects identified for the renal cortex samples were physiological normal with relevant signs of physiological function (structural integrity, specific cellular distribution, intensively vascularized regions), indicating thus either that the AgNPs are not suitable for renal excretion or that the silver-based particles have already been eliminated (in case that the AgNPs have extremely reduced dimensions and do not form agglomerate structures).

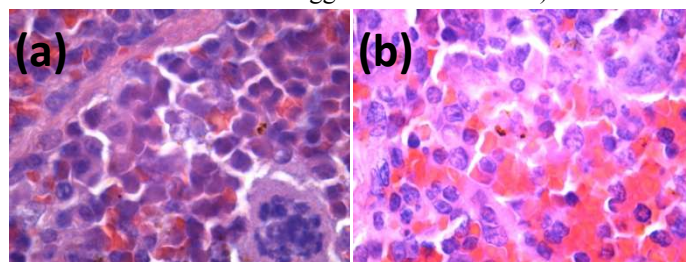


Figure 6. Histological features of splenic tissue (a,b) harvested after 14 days of treatment with AgNPs. H&E staining, $1000\times$ magnification.

When considering the histological aspects corresponding to the splenic tissue (Figure 6), one could clearly notice significant histological modifications, after both experimental treatments. Due to an intense immune system activity required during the formation of multi-lobed macrophages within the splenic tissue, one can notice the significant hypertrophy of the splenic white pulp. The endothelial cells with prominent spherical-ellipsoidal shaped nuclei within the splenic red pulp cellular cords specifically delimit the splenic capillaries. Within this splenic region one can observe significant dark brown agglomerate deposits. The identified aggregate structures have spherical morphology and variable dimensions (below $3 \mu\text{m}$) and are specifically located within the macrophage system cells which belong both to Billroth cords and sinusoid capillaries. The aggregate structures with micronic dimensions were associated with the formation of AgNPs-based deposits within the spleen. It is also important to mention that the inorganic granular structures seemed to have a reduced significance and distribution after 14 days treatment (when compared to 7 days of treatment), suggesting thus the efficiency of the immune system and the possibility to completely eliminate the AgNPs-based deposits in long time periods.

3.9. Modulation of bacterial biofilms development

The anti-bacterial activity and anti-biofilm potential of the AgNPs-coated medical devices were assessed against three selected bacterial strains, after various periods of incubation. The

uncoated catheter sections used as control revealed higher colony forming units (CFU) of *E. coli* per mL after 24, 48 and 72 hours of incubation, i.e.: $1.1 \cdot 10^6$, $1.4 \cdot 10^6$, respectively $1.9 \cdot 10^6$ CFU/mL. The modified catheter sections strongly inhibited the *E. coli* bacterial colonization, the CFU/mL reported values being significantly reduced to: $0.6 \cdot 10^5$, $1.10 \cdot 10^5$ and $1.2 \cdot 10^5$ CFU/mL, respectively. Thus, one can conclude that the AgNPs-based coatings exhibit a strong anti-biofilm potential against *E. coli* bacterial strain, the CFU/mL values being significantly reduced (with approx. 90%) in the presence of the experimentally modified catheter sections (when compared to control uncoated catheter sections).

The control catheter sections treated with *S. aureus* bacterial strain recorded a high microbial charge, the CFU/mL values being of $1.6 \cdot 10^6$ (24 h), $1.85 \cdot 10^6$ (48 h) and $1.4 \cdot 10^7$ (72 h). When considering the experimentally modified medical devices, a reduced bacterial colonization was observed, i.e., $0.9 \cdot 10^5$

4. CONCLUSIONS

The promising results regarding higher and longer resistance to bacterial contamination, as well as good

CFU/mL, $1.08 \cdot 10^6$ CFU/mL and $1.2 \cdot 10^6$ CFU/mL, respectively. Although the anti-biofilm activity was lower in case of the Gram-positive *S. aureus* when compared to *E. coli*, however the CFU/mL were reduced with approx. 60% (when compared to control assays), confirming thus the efficiency of the modified medical devices against *S. aureus* biofilm.

In case of *P. aeruginosa*, one of the most reputed opportunistic pathogens implicated in medical devices associated infections, a microbial load of $1.7 \cdot 10^6$, $1.9 \cdot 10^6$ and $1.2 \cdot 10^7$ CFU/mL was reported after 24, 48, respectively 72 hours of incubation with uncoated catheter sections. In the presence of AgNPs-coated medical devices only a slightly reduced bacterial contamination was noticed, i.e., $1.1 \cdot 10^5$, $1.1 \cdot 10^6$ and $1.4 \cdot 10^6$ CFU/mL, revealing a lower inhibitory activity of the silver-based coated catheter sections against this pathogen, as compared to the previously discussed ones.

biocompatibility reveal the potential of the MAPLE technique for optimizing the surface of day-to-day medical care devices.

5. REFERENCES

- [1] Revdiwala S., Rajdev B.M., Mulla S., Characterization of Bacterial Etiologic Agents of Biofilm Formation in Medical Devices in Critical Care Setup, *Critical Care Research and Practice*, **2012**.
- [2] Welte T., Nosocomial Infections – a Present and Future Challenge, *Deutsches Ärzteblatt International*, 110, 30, 625-626, **2013**.
- [3] Chen M., Yu Q., Sun H., Novel Strategies for the Prevention and Treatment of Biofilm Related Infections, *International Journal of Molecular Sciences*, 14, 18488-18501, **2013**.
- [4] Chen L., Wen Y., The role of bacterial biofilm in persistent infections and control strategies, *International Journal of Oral Science*, 3, 66-73, **2011**.
- [5] Lee H.S., Kim Y.W., Kim J.E., Yoon S.W., Kim T.Y., Noh J.S., Suh K.S., Synthesis of dimension-controlled silver nanowires for highly conductive and transparent nanowire films. *Acta Materialia*, 83, 84-90, **2015**.
- [6] Park M., Sohn Y., Shin W.G., Lee J., Ko S.H., Ultrasonication assisted production of silver nanowires with low aspect ratio and their optical properties. *Ultrasonics Sonochemistry*, 22, 35-40, **2015**.
- [7] Mashentseva A., Borgekov D., Kislitsin S., Zdorovets M., Migunova A., Comparative catalytic activity of PET track-etched membranes with embedded silver and gold nanotubes, *Nuclear Instruments and Methods in Physics Research Section B: Beam Interactions with Materials and Atoms*, **2015**.
- [8] Yang A., Li X., Guo P., Vibrational properties of single-walled silver nanotubes studied from first principles, *Physica E: Low-dimensional Systems and Nanostructures*, 74, 310-317, **2015**.
- [9] Bahemmat S., Ghassemzadeh M., Neumüller B., A new silver(I) coordination polymer containing 3-methylthio-(1H)-1,2,4-triazole as precursor for preparation of silver nanorods, *Inorganica Chimica Acta*, 435, 159-166, **2015**.
- [10] Liaw J.W., Li W.J., Lin W.C., Kuo M.K., Theoretical study of optical torques for aligning Ag nanorods and nanowires, *Journal of Quantitative Spectroscopy and Radiative Transfer*, 162, 133-142, **2015**.
- [11] Deng C., Zhang X., Cai H., Green synthesis of monodisperse silver nanoparticles using hydroxy propyl methyl cellulose, *Journal of Alloys and Compounds*, 583, 267-271, **2014**.
- [12] Pyne S., Samanta S., Misra A., Photochemical synthesis of Ag nanobars and their potential application as catalyst, *Solid State Sciences*, 26, 1-8, **2013**.
- [13] Behra R., Sigg L., Clift M.J.D., Herzog F., Minghetti M., Johnston B., Petri-Fink A., Rothen-Rutishauser B., Bioavailability of silver nanoparticles and ions: from a chemical and biochemical perspective, *Journal of the Royal Society Interface*, **2013**.
- [14] Zhang T., Song Y.J., Zhang X.Y., Wu J.Y., Synthesis of Silver Nanostructures by Multistep Methods, *Sensors*, 14, 5860-5889, **2014**.
- [15] El-Nour K.M.M.A., Eftaiha A., Al-Warthan A., Ammar R.A.A., Synthesis and applications of silver nanoparticles, *Arabian Journal of Chemistry*, 3, 135-140, **2010**.
- [16] Sergeev G.B., Klabunde K.J., Synthesis and Stabilization of Nanoparticles, *Nanochemistry* (Second Edition), ed. Elsevier, 11-43, **2013**.
- [17] Ashraf S., Abbasi A.Z., Pfeiffer C., Hussain S.Z., Khalid Z.M., Rivera Gil P., Parak W.J., Hussain I., Protein-mediated synthesis, pH-induced reversible agglomeration, toxicity and cellular interaction of silver nanoparticles, *Colloids and Surfaces B: Biointerfaces*, 102, 511-518, **2013**.
- [18] Khan Z., Hussain J.I., Hashmi A.A., Al-Thabaiti S.A., Preparation and characterization of silver nanoparticles using aniline, *Arabian Journal of Chemistry*, **2013**.
- [19] Zhao X., Xi Y., Li Q., Ma X., Quan F., Geng C., Han Z., Microwave-assisted synthesis of silver nanoparticles using sodium alginate and their antibacterial activity, *Colloids and Surfaces A: Physicochemical and Engineering Aspects*, 444, 180-188, **2014**.
- [20] Akhavan A., Sheikh N., Khoylou F., Naimian F., Ataievarjovi E., Synthesis of antimicrobial silver/hydroxyapatite nanocomposite by gamma irradiation, *Radiation Physics and Chemistry*, 98, 46-50, **2014**.
- [21] Aswathy B., Avadhani G.S., Sumithra I.S., Suji S., Sony G., Microwave assisted synthesis and UV-Vis spectroscopic studies of silver nanoparticles synthesized using vanillin as a reducing agent, *Journal of Molecular Liquids*, 159, 165-169, **2011**.
- [22] Darroudi M., Zak A.K., Muhamad M.R., Huang N.M., Hakimi M., Green synthesis of colloidal silver nanoparticles by sonochemical method, *Materials Letters*, 66, 117-120, **2012**.
- [23] Krajczewski J., Joubert V., Kudelski A., Light-induced transformation of citrate-stabilized silver nanoparticles: Photochemical method of increase of SERS activity of silver colloids, *Colloids and Surfaces A: Physicochemical and Engineering Aspects*, 456, 41-48, **2014**.
- [24] Yahyaie B., Azizian S., Rapid photogeneration of silver nanoparticles in ethanolic solution: A kinetic study, *Spectrochimica Acta Part A: Molecular and Biomolecular Spectroscopy*, 101, 343-348, **2013**.
- [25] Ibrahim H.M.M., Green synthesis and characterization of silver nanoparticles using banana peel extract and their antimicrobial activity against representative microorganisms, *Journal of Radiation Research and Applied Sciences*, **2015**.
- [26] Mallikarjuna K., Sushma N.J., Narasimha G., Manoj L., Raju B.D.P., Phytochemical fabrication and characterization of silver nanoparticles by

using Pepper leaf broth, *Arabian Journal of Chemistry*, 7, 6, 1099-1103, **2014**.

[27] Raut R.W., Mendhulkar V.D., Kashid S.B., Photosensitized synthesis of silver nanoparticles using With an iasomnifera leaf powder and silver nitrate, *Journal of Photochemistry and Photobiology B: Biology*, 132, 45-55, **2014**.

[28] Ahmad T., Wani I.A., Manzoor N., Ahmed J., Asiri A.M., Biosynthesis, structural characterization and antimicrobial activity of gold and silver nanoparticles, *Colloids and Surfaces B:Biointerfaces*, 107, 227-234, **2013**.

[29] El-Raheem A., El-Shanshoury R., El-Silk A.E., Ebeid M.E., Extracellular Biosynthesis of Silver Nanoparticles Using Escherichia coli ATCC 8739, Bacillus subtilis ATCC 6633, and Streptococcus thermophilus ESh1 and Their Antimicrobial Activities, *ISRN Nanotechnology*, **2011**.

[30] Kalpana D., Lee Y.S., Synthesis and characterization of bactericidal silver nanoparticles using cultural filtrate of simulated microgravity grown Klebsiella pneumonia, *Enzyme and Microbial Technology*, 52, 151-156, **2013**.

[31] Singh D., Rathod V., Ninganagouda S., Herimath J., Kulkarni P., Biosynthesis of silver nanoparticle by endophytic fungi Pencillium sp. isolated from Curcuma longa (turmeric) and its antibacterial activity against pathogenic gram negative bacteria, *Journal of Pharmacy research*, 7, 448-453, **2013**.

[32] Bozaci E., Akar E., Ozdogan E., Demir A., Altinisik A., Seki Y., Application of carboxymethylcellulose hydrogel based silver nanocomposites on cotton fabrics for antibacterial property, *Carbohydrate Polymers*, 134, 128-135, **2015**.

[33] Srivatsan K.V., Duraipandy N., Begum S., Lakra R., Ramamurthy U., Korrapati P.S., Kiran M.S., Effect of curcumin caged silver nanoparticle on collagen stabilization for biomedical applications, *International Journal of Biological Macromolecules*, 75, 306-315, **2015**.

[34] Zhao X., Li Q., Ma X., Quan F., Wang J., Xia Y., The preparation of alginate-AgNPs composite fiber with green approach and its antibacterial activity, *Journal of Industrial and Engineering Chemistry*, 24, 188-195, **2015**.

[35] Damelin L.H., Fernandes M.A., Tiemessen C.T., Alginate microbead-encapsulated silver complexes for selective delivery of broad-spectrum silver-based microbicides, *International Journal of Antimicrobial Agents*, 46, 394-400, **2015**.

[36] Guo D., Zhang J., Huang Z., Jiang S., Gu N., Colloidal silver nanoparticles improve anti-leukemic drug efficacy via amplification of oxidative stress, *Colloids and Surfaces B:Biointerfaces*, 126, 198-203, **2015**.

[37] Yadollahi M., Farhoudian S., Namazi H., One-pot synthesis of antibacterial chitosan/silver bio-nanocomposite hydrogel beads as drug delivery systems, *International Journal of Biological Macromolecules*, 79, 37-43, **2015**.

[38] Hong M.L., Li L.J., Han H.X., Chu X., A Label-free Fluorescence Assay for Trypsin Based on the Electron Transfer between Oligonucleotide-stabilized Ag Nanoclusters and Cytochrome C, *Analytical Science*, 30, 811-815, **2014**.

[39] Ma H., Song K., Zhou L., Zhao X., A Naked Eye Refractive Index Sensor with a Visible Multiple Peak Metamaterial Absorber, *Sensors*, 15, 7454-7461, **2015**.

[40] Zhang Y., Gao G., Liu H., Fu H., Fan J., Wang K., Chen Y., Li B., Zhang C., Zhi X., He L., Cui D., Identification of Volatile Biomarkers of Gastric Cancer Cells and Ultrasensitive Electrochemical Detection based on Sensing Interface of Au-Ag Alloy coated MWCNTs, *Theranostics*, 4, 2, 154-162, **2014**.

[41] Braun, G.B. Friman T., Pang H.B., Pallaoro A., Hurtado de Mendoza T., Willmore A.M.A., Kotamraju V.R., Mann A.P., She Z.G., Sugahara K.N., Reich N.O., Teesalu T., Ruoslahti E., Etchable plasmonic nanoparticle probes to image and quantify cellular internalization, *Nature Materials*, 13, 9, 904-911, **2014**.

[42] Gao S., Chen D., Li Q., Ye J., Jiang H., Amatore C., Wang X., Near-infrared fluorescence imaging of cancer cells and tumors through specific biosynthesis of silver nanoclusters, *Scientific Reports*, 4, 4384, **2014**.

[43] Zou J., Hannula M., Misra S., Feng H., Labrador R.H., Aula A.S., Hyttinen J., Pyykkö I., Micro CT visualization of silver nanoparticles in the middle and inner ear of rat and transportation pathway after transtympanic injection, *Journal of Nanobiotechnology*, 13, 5, **2015**.

[44] Eraković S., Janković A., Ristoscu C., Duță L., Șerban N., Vișan A., Mihăilescu I.N., Stan G.E., Socol M., Iordache O., Dumitrescu I., Luculescu C.R., Janácković Dj., Mišković-Stanković V., Antifungal activity of Ag:hydroxyapatite thin films synthesized by pulsed laser deposition on Ti and Ti modified by TiO₂ nanotubes substrate, *Applied Surface Science*, 293, 37-45, **2014**.

[45] González-Sánchez M.I., Perni S., Tommasi G., Morris N.G., Hawkins K., López-Cabarcos E., Prokopovich P., Silver nanoparticle based antibacterial methacrylate hydrogels potential for bone graft applications, *Materials Science and Engineering: C*, 50, 332-340, **2015**.

[46] Piccirillo C., Pullar R.C., Tobaldi D.M., Lima Castro L.M., Estevez Pintado M.M., Silver-containing calcium phosphate materials of marine origin with antibacterial activity, *Ceramics International*, 41, 10152-10159, **2015**.

[47] Challener C., The Intelligence Behind Smart Coatings, *JCT Coatings Tech*, 50-55, **2006**.

[48] Wang G., Zreiqat, H., Functional Coatings or Films for Hard-Tissue Applications, *Materials*, 3, 3994-4050, **2010**.

[49] Mariselvam R., Ranjitsingh A.J.A., Nanthini A.U.R., Kalirajan K., Padmalatha C., Selvakumar P.M., Green synthesis of silver nanoparticles from the extract of the inflorescence of Cocos nucifera (Family: Arecaceae) for enhanced antibacterial activity, *Spectrochimica Acta Part A: Molecular and Biomolecular Spectroscopy*, 129, 537-541, **2014**.

[50] Perni S., Hakala V., Prokopovich P., Biogenic synthesis of antimicrobial silver nanoparticles capped with L-cysteine, *Colloids and Surfaces A: Physicochemical and Engineering Aspects*, 460, 219-224, **2013**.

[51] Van Dong P., Ha C.H., Binh L.B., Kasbohm J., Chemical synthesis and antibacterial activity of novel-shaped silver nanoparticles, *International Nano Letters*, 2, 9, **2012**.

[52] Mihaiescu D.E., Grumezescu A.M., Andronescu E., Voicu G., Ficai A., Vasile O.R., Bleotu C., Saviuc C., Prosthetic Devices with Functionalized antibiofilm surface based NanoAg@C18, *Current Organic Chemistry*, 17, 2, 105-112, **2013**.

[53] Fufă M.O.M., Grumezescu A.M., Part II – New strategy to control microbial infections, *Bioactive and nanostructured surfaces - New strategies to control microbial infections*, Lambert Academic Publishing, 44-71, **2015**.

6. ACKNOWLEDGEMENTS

The work has been funded by the Sectoral Operational Programme Human Resources Development 2007-2013 of the Ministry of European Funds through the Financial Agreement POSDRU/156/1.2/G/135764 (ChimMaster).

© 2015 by the authors. This article is an open access article distributed under the terms and conditions of the Creative Commons Attribution license (<http://creativecommons.org/licenses/by/4.0/>).